Coaxial Thermoplastic Elastomer-Wrapped Carbon Nanotube Fibers for Deformable and Wearable Strain Sensors

Coaxial Thermoplastic Elastomer-Wrapped Carbon Nanotube Fibers for Deformable and Wearable Strain Sensors

Jian Zhou, Xuezhu Xu, Yangyang Xin, and Gilles Lubineau**

Highly conductive and stretchable fibers are crucial components of wearable electronics systems. Excellent electrical conductivity, stretchability, and wearability are required from such fibers. Existing technologies still display limited performances in these design requirements. Here, achieving highly stretchable and sensitive strain sensors by using a coaxial structure, prepared via coaxial wet spinning of thermoplastic elastomer-wrapped carbon nanotube fibers, is proposed. The sensors attain high sensitivity (with a gauge factor of 425 at 100% strain), high stretchability, and high linearity. They are also reproducible and durable. Their use as safe sensing components on deformable cable, expandable surfaces, and wearable textiles is demonstrated.

Q3

1. Introduction

Stretchable conductors are crucial components of wearable electronics, flexible displays, transistors, mechanical sensors, and energy devices.[1–7] Stretchable fiber conductors are very promising for the next generation of wearable electronics because they can be easily produced in large quantities and easily woven into fabrics.[8–12] Recently, stretchable fibers have evolved toward high stretchability, and high sensitivity to adapt to applications like e-skins, and health monitoring systems.[8,13,14]

The main parameters responsible for the quality of the performance of strain sensors are sensitivity, stretchability, and linearity. The sensitivity (defined by the gauge factor, GF) is expressed by the relative change in resistance versus the strain. The stretchability is the maximum uniaxial tensile strain of the sensor before it breaks. The linearity quantifies how constant the GF is over the measurement range. Good linearity makes the calibration process easier and ensures accurate measurements throughout the whole range of applied strains. However, strain sensors based on conventional fiber cannot combine high sensitivity (GF > 100), high stretchability (strain >100%), and high linearity.[13] Carbonized silk fiber was used as a component in wearable strain sensors with a good stretchability.[15] However, the sensitivity of the sensor was low and the GF increased from 9.6 to 37.5 as the strain is increased from 250% to 500%, showing a large change over the strain measurement range. Graphene-based composite fibers with "compression ring" architecture increased a sensor's stretchability, but the architecture of the sensor was very complex and its GF was low (GF = 1.5 at 200% strain).[12] An electronic fabric based on intertwined electrodes with piezoresistive rubber simultaneously mapped and quantified mechanical strain, but the fabrication process was very complex and time-consuming.[16]

One versatile approach for the industrial fabrication of continuous fibers that has been used for many decades is wet-spinning. It provides a robust route for engineering high-performance conductive fibers.[8,10,17–20] Previously, a silver nanoparticle/thermoplastic elastomer (TPE) mixture was wet-spun to construct microfiber-based strain sensors, but it was challenging to maintain a continuous conductive path in the fibers and a homogeneous distribution of the metallic fillers.[21] Conductive polymer/thermoplastic elastomer fiber was also prepared by wet-spinning for highly stretchable sensors, but it was difficult to maintain both stretchability and sensitivity, even with high loading of the conductive polymer fillers.[22,23] In our previous study, conductive poly(3,4-ethylene-dioxythiophene)/poly(styrene sulfonate) (PEDOT/PSS) polymer microfibers were fabricated via hot-drawing-assisted wet-spinning. We achieved an electrical conductivity of 2804 S cm^{-1}, which was accomplished by combining the vertical hot-drawing process with solvent doping and dedoping of the microfibers. Due to the brittle nature of PEDOT/PSS, the stretchability of the conductive fiber was limited to 20% and the GF was only 1.8 at 13% strain.[17] The wet-spinning process has also been successfully applied to make single-walled carbon nanotube (SWCNT) microwires for strain sensors with a high GF of 10^5, though the stretchability was limited to 15%.[24] Most of the aforementioned sensors show a large nonlinearity.[13] Moreover, the conductive surface of the fibers is exposed in most of these sensors, so they carry with them the risk of short circuiting when used as strain sensors. The consequence is poor stability and durability. As a result, a new generation of conductive and stretchable fibers is needed for designing high-performance strain sensors.

Here, we combined the coaxial wet-spinning approach with a posttreatment process to prepare TPE-wrapped SWCNT fibers

J. Zhou, X. Xu, Y. Xin, G. Lubineau
Physical Sciences and Engineering Division
COHMAS Laboratory
King Abdullah University of Science and Technology (KAUST)
Thuwal 23955-6900, Saudi Arabia
E-mail: jian.zhou@kaust.edu.sa; gilles.lubineau@kaust.edu.sa

Q2

The ORCID identification number(s) for the author(s) of this article can be found under https://doi.org/10.1002/adfm.201705591.

DOI: 10.1002/adfm.201705591

for use in high-performance strain sensors. The as-spun fibers containing SWCNT/acid dope in their core were posttreated in an acetone bath to remove acid residue and the SWCNT core was densified by pressing on the surface of the fibers, leading to a belt-like coaxial fiber. The fibers fragment with a high density of cracks when stretching above their crack-onset strain. The entangled networks of SWCNTs bridging the cracked fragments play a key role during the strain sensing. We evaluate these coaxial fibers as high-performance strain sensors and demonstrate their capabilities as deformable and wearable electronics.

2. Results and Discussion

2.1. Coaxial Thermoplastic Elastomer-Wrapped SWCNT Fibers

Figure 1a shows an illustration of the coaxial wet-spinning and posttreatment process for making the fibers. The spinning nozzle has the coaxial inner and outer channels, respectively. The inner spinning dope was 2 wt% SWCNT/CH_3SO_3H. The CH_3SO_3H acted as a dispersing agent for the highly concentrated SWCNTs, so that the dope could be spun into the continuous microwires according to a previously reported dispersing and wet-spinning method.[17–19,24,25] The solution of TPE in CH_2Cl_2 was selected as the outer spinning solution because TPE is an electrically insulative elastomer. This polymer sheath protected the fiber electrodes from short circuiting and environmental degradation. Also, as an ultrastretchable substrate, it introduced remarkable stretchability to the conductive coaxial fibers. The SWCNT/CH_3SO_3H dope from the inner channel and the TPE/CH_2Cl_2 solution from the outer channel were introduced into the ethanol coagulation bath simultaneously. The ethanol bath extracted the CH_2Cl_2 from the TPE/CH_2Cl_2 dope, while theCH_3SO_3H still remained in the SWCNT core. A single TPE-wrapped SWCNT coaxial fiber was then wet-spun and collected successfully with a length of more than 5 m (Figure 1b), showing the potential of these fibers for large-scale production. Due to the high boiling point of CH_3SO_3H (167° C) and the quick solidification of TPE in the ethanol bath, most

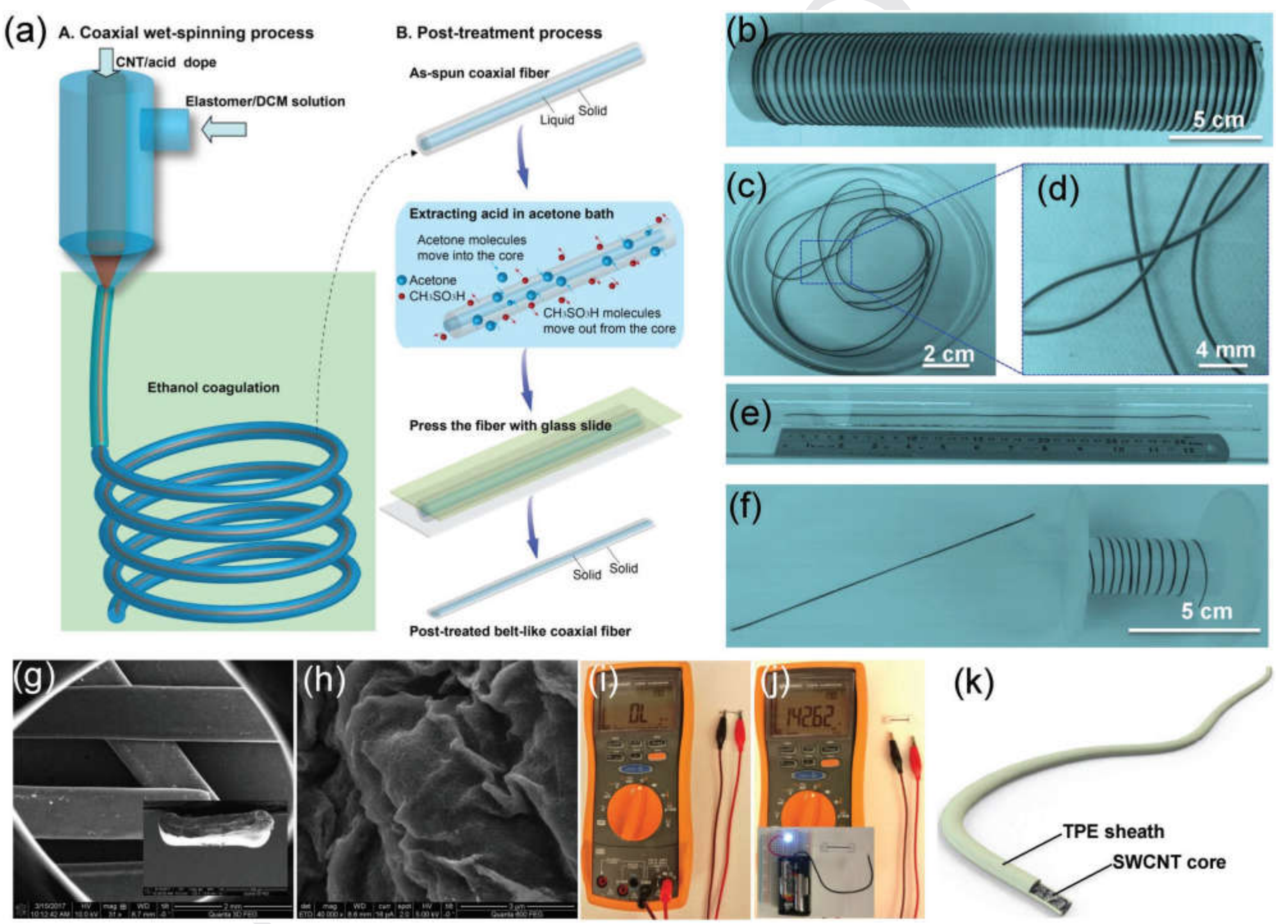

Figure 1. Conductive coaxial fibers. a) Schematic of the coaxial wet-spinning and posttreatment process for producing the fibers. b) A single as-spun fiber was collected on a continuously winding drum spool. The length of the fiber was over 5 m. c,d) The as-spun fiber was immersed in acetone to extract CH_3SO_3H. e) The fiber was pressed to obtain a densified and compact structure. f) A single coaxial fiber after posttreatment process also collected on a winding spool. g) SEM image of the coaxial wet-spun fiber showing a belt-like structure. The inset shows the cross-section image of the fiber. The thickness and width were 200 and 1050 µm, respectively. h) The SEM image shows randomly oriented networks in the SWCNT core after the TPE sheath was removed by CH_2Cl_2. i,j) Initial electrical measurements taken on the surface and in the core of the coaxial fiber. Inset image in (j) shows an LED light by a coaxial fiber with a length of 2 cm at 3 V. k) Schematic presenting the core–sheath structure of the fiber.

of the acid still remained in the core even after the fiber was collected. In the posttreatment process, the acid was removed from the SWCNT core by immersing the fiber in an acetone bath, as shown in Figure 1a,c,d. The extraction was monitored by observing the diameter of the fiber. As shown in Figure S1a,b (Supporting Information), the fiber diameter decreased with a longer extraction time. This is associated with the removal of the acid and not with the dissolution of the TPE by acetone. Indeed, in a preliminary experiment, we found that after mixing 20 wt% of TPE in acetone for 2 h, a white suspension formed that separated into two layers after 10 min. Even pure TPE fibers retain their fiber structure after immersion them in acetone for 6 h (Figure S2a– c). Moreover, the FTIR spectrum of the TPE fiber did not change after washing in acetone for 6 h (Figure S2d, Supporting Information). These results suggest that acetone did not significantly modify the TPE in the 6 h posttreatment. The PH value of desiccated fibers also depended on the extraction time. After taking the fiber out of the acetone bath, evaporation of the acetone residue resulted in an uneven surface (Figure S1c, Supporting Information). Therefore, the fiber was pressed into a belt-like shape with a glass slide, as shown in Figure 1e–g. The resulting thickness and width were 200 and 1050 µm, respectively, as measured from the scanning electron microscopy (SEM) image (Figure 1g). To investigate the morphology of the SWCNTs in the core, the TPE layer was dissolved in CH_2Cl_2. The porous structure of the SWCNT layer with randomly distributed SWCNT networks can be observed in the SEM image (Figure 1h). Some SWCNTs joined together and formed larger bundles, which played an important role in reducing the overall resistance of the fiber. Figure 1i shows that the coaxial fiber acted as an insulator when measured on its surface, due to the protection of the insulative TPE sheath. After connecting the 2 cm long SWCNT core with silver paste and copper wire (Figure S3, Supporting Information), the fiber was measured to have a low resistance of 142.6 Ω (Figure 1j). We displayed the electrical function of the fibers by connecting a light-emitting diode (LED) with one coaxial fiber. The resistance of the fiber was very low, even able to light the LED at 3 V, as demonstrated in the inset of Figure 1i. Thus, we confirmed that the conductive coaxial fiber made of a TPE-wrapped SWCNT core was achieved through the wet-spinning and posttreatment process (Figure 1k). The successful production of these coaxial fibers will be key for their adoption in wearable electronics.

2.2. Crack Opening in the Coaxial Fiber

Figure 2a,b shows the incremental cyclic loading and unloading curves of a pure TPE fiber and a coaxial fiber at a rate of 5 cm min^{-1}. After the first cycle (0% to 50% strain), both of the curves show that there is a 10–15% residual strain that is negligible deformation compared with the total deformation in the following cycles. Figure 2a shows the typical mechanical behavior of pure TPE, which could extend far with a good elastic recovery.[26] Compared to pure TPE, the coaxial fibers experienced a sharp stress increase during the first loading cycle. The Young's modulus calculated from the first loading cycle was 112 MPa, 24 times higher than that of pure TPE fiber (4.5 MPa), suggesting that the SWCNT core increased the Young's modulus of TPE. The SWCNT core of the coaxial fiber became fragmented during loading, as indicated in Figure 2b,c. This is evidence of good stress transfer between the TPE matrix and the SWCNT core.

Figure 2d depicts the development of cracks in a typical coaxial fiber under an optical microscope. As the fiber stretched, the crack opening displacement, L_c, correlated almost linearly

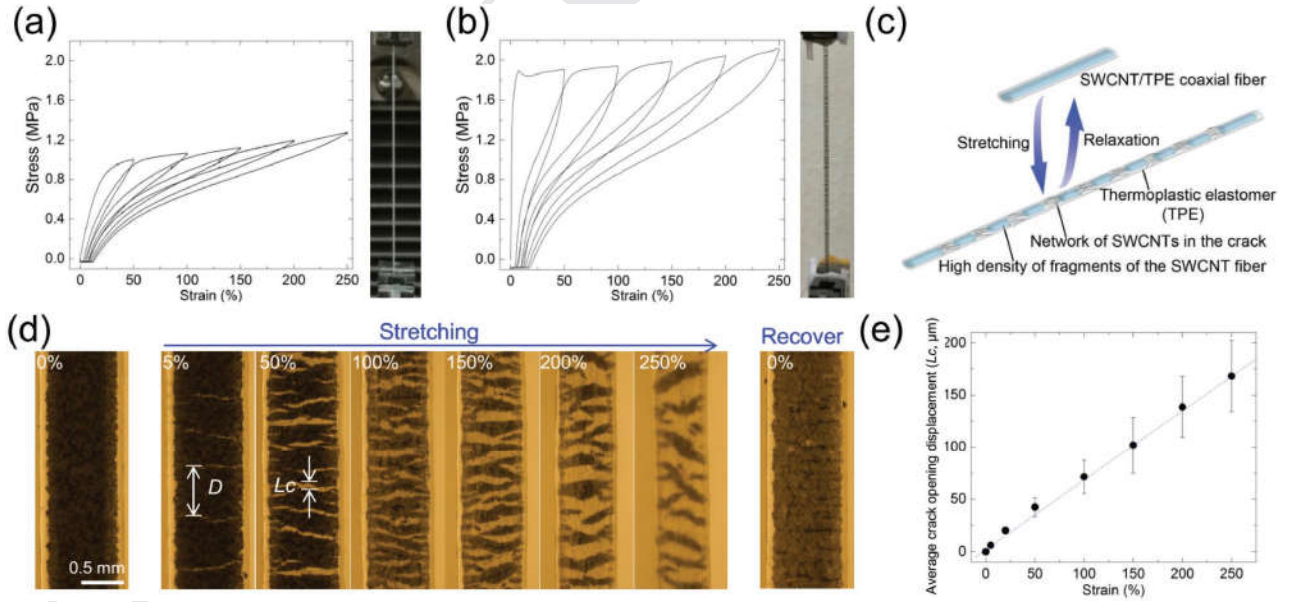

Figure 2. Opening of cracks in the coaxial fiber. a,b) Incremental cyclic loading and unloading tests on a pure TPE fiber and a coaxial fiber from 50% to 250% strain at a rate of 5 cm min^{-1}. The photo on the right side of each figure shows the loading state at 100% strain of the pure TPE fiber and the coaxial fiber, respectively. c) Schematic presenting the fragmentation of the coaxial fiber. d) Images of a typical coaxial fiber when stretched from 0% to 250% strain, and relaxation after unloading. *D* and L_c represent the average spacing between the cracks and average crack opening displacement, respectively. e) Evolution of the average crack opening displacement, L_c, on the applied strain from 0% to 250%.

to the applied strain (Figure 2e), proving the overall elastic behavior of the fiber. When the applied strain increased from 0% to 250%, the resistance of the fiber increased from 142 Ω to 2.3 MΩ. Cracks appeared perpendicular to the loading direction ($\varepsilon < 50\%$), and then multiplied along a quasi-periodical network as the strain grew larger ($\varepsilon > 50\%$). The crack density, $1/D$, was found to be 17 mm^{-1}, remarkably higher than found in previous studies of SWCNT wires or thin paper in PDMS substrate.[24,25,27] Such a high crack density is vital to increasing the stretchability and linearity of the resistance response of the fibers during stretching. Compared to the initial state at 0% strain, the cracks nearly recovered completely after unloading, with small but observable openings. The resistance of the stretched fiber was measured to be 1.5 kΩ, ten times that of the original fiber. This is ascribed to the unrecoverable conductive paths in the SWCNT core, as shown in Figure 2d.

2.3. Strain Sensing

Figure 3a presents the change in resistance of a coaxial fiber with strains from 0% to 250%, corresponding to the incremental stress–strain curves in Figure 2b. The resistance clearly increased with strain. After unloading from the 250% strain, the fragmented structure of the coaxial fiber with a high crack density of 17 mm^{-1} could be used as the sensing component in strain sensors. We performed repetitive cyclic testing on the fibers at lower strains (0% to 100% strain), which may be more representative of strains encountered in real applications (e.g., wearable electronics). Figure S4b (Supporting Information) shows that after the first cyclic test (0% to 100% strain), the subsequent cycles overlapped with minimal signs of hysteresis. Figure 3b shows five cycles of a strain ranging from 0% to 100%, during which the resistance

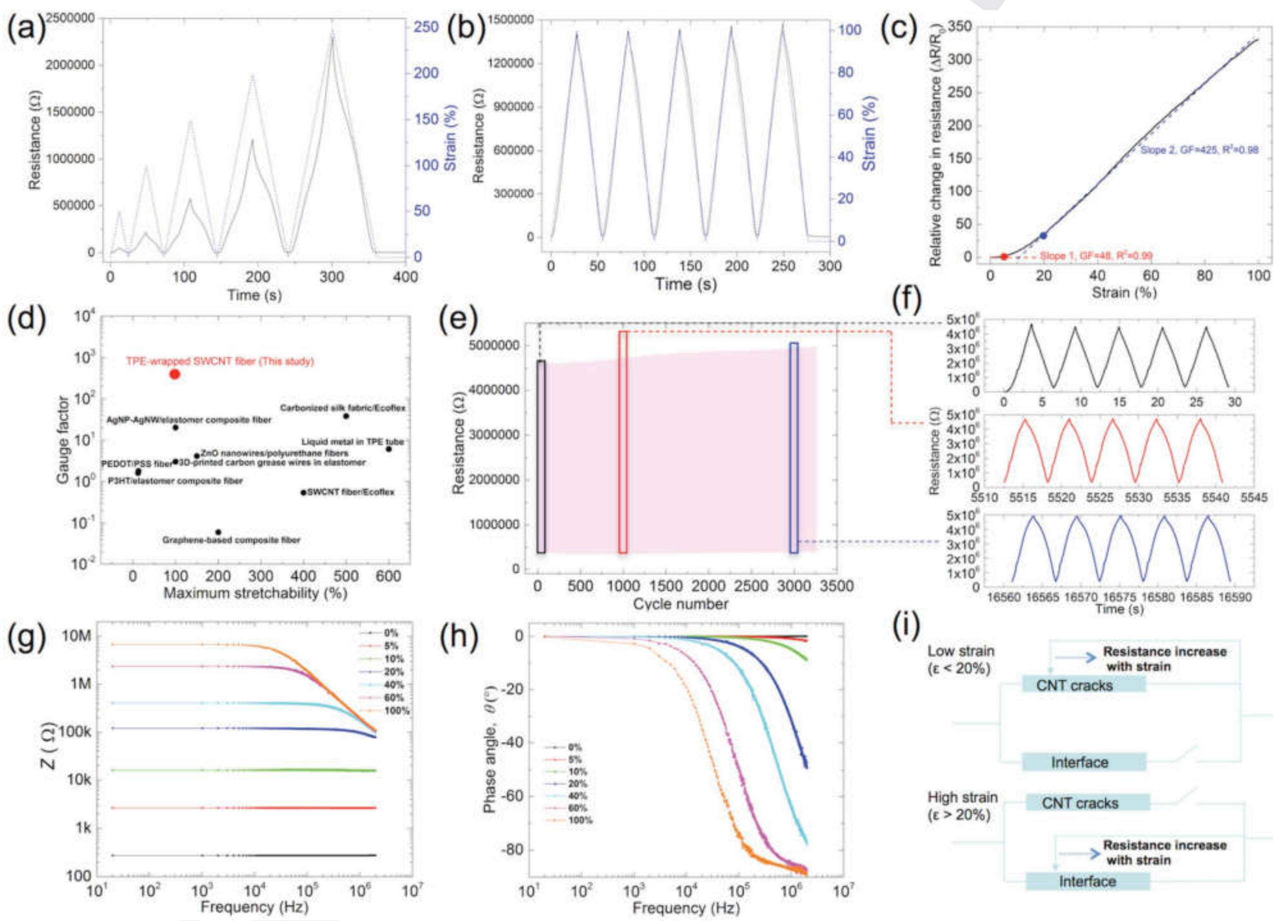

Figure 3. Strain sensing of the coaxial fiber. a) Electrical resistance changes under incremental cyclic loading and unloading of a coaxial fiber, which correspond to the stress-strain curve in Figure 2b. b) Dynamic response of the fiber-based strain sensors to five loading and unloading cycles at 100% strain. c) Relative change in resistance versus strain on the fiber. Red and blue represent the fitting lines for the applied strain from 0% to 5% (with a linearity of 0.99), and the applied strain from 20% to 100% (with a linearity of 0.98), respectively. d) GFs as a function of the maximum stretchability of recently studied fiber-based strain sensors.[9,12,17,21,22,28,29] e) Dynamic response of the fiber to stretching and relaxing cycles from 20% to 100% strain at a rate of 400 mm min^{-1}, showing long-term repeatability of the sensor after 3250 cycles. f) Repeatability of the fiber sensor at cycles 1–5, 1000–1005, and 3000–3005, as indicated in (e). g,h) Electrical impedance spectroscopy of the fiber-based strain sensor at different applied strains showing the frequency dependencies of the moduli of the complex impedance (Z) and phase angle (θ), respectively. i) Schematic shows the equivalent circuit model of the strain sensor response to applied strain.

of the fiber progressed along a very reversible course, closely following the change in the applied strain.

To determine the sensitivity of the fiber, we show the relative change in resistance ($\Delta R/R_0$) with the applied strain in Figure 3c. R_0 is the initial resistance after the first stretch to 250% strain. The change in resistance of this coaxial fiber was $\Delta R/R_0 = 340$ at the 100% strain. The sensing performance of the fiber-based sensor featured two linear regions with two slopes (the applied strain from 0% to 5% with a linearity of 0.99, and the applied strain from 20% to 100% with a linearity of 0.98), which reflect the GF at different strain ranges: the GF was 48 at 0–5% strain and 425 at 20–100% strain. However, conventional metal gauges have a GF of only around 2.0 at strains less than 5%.[3,13] The GF was higher than those of other fiber-based strain sensors (Figure 3d).[9,12,15,17,21,22,28,29] Piezoresistive strain sensors often can reach a high GF or high stretchability, but normally with hysteresis and nonlinearity.[13] Figure 3e shows that our sensor had good durability and reproducibility, which are important for long-term use. After 3250 cycles of stretching and relaxing from 20% to 100% strain, the performance of the strain sensor remained repeatable. The good repeatability of the sensor was confirmed at cycles 1–5, 1000–1005, and 3000–3005 (Figure 3f).

In order to elucidate the sensing mechanism of the sensor made with coaxial fibers, we performed a characterization of the electrical impedance response to a wide range of frequencies. Figure 3g,h displays the frequency dependencies of the moduli of the complex impedance (Z) and phase angle (θ), respectively. Figure 3i shows an equivalent circuit model, generated from the electrical impedance spectroscopy (EIS) results, that captures the behavior of the coaxial fiber at different strain levels. At low strain ($\varepsilon < 20\%$), the impedance was almost constant in the tested frequency range and the conduction mechanism was expressed by the resistive behavior of the SWCNT in the core. The many redundant contacts among the SWCNTs in the crack regions ensured macroscopic ohmic behavior in the low-strain regime. The resistance of the SWCNT core progressively increases with the strain during stretching due to the opening of the cracks (Figure 2b–d). At higher strain ($\varepsilon > 20\%$), the impedance (Z) became more dependent on frequency (Figure 3g). Indeed, as the strain continued to increase, the SWCNTs became increasingly disconnected. The conduction of electrons through the SWCNT cracks in the core rapidly became impossible. Consequently, these cracks were considered open circuits (Figure 3i). The only conduction path is now the SWCNT-covered interface in the TPE sheath. We ascribed the increase in resistance with the strain to the progressive stretching of the SWCNT network covering the TPE sheath in the delaminated area. The change in phase from 0° to −90° suggests that the junctions macroscopically behave like a parallel resistor and capacitor. The capacitive part increased with the amount of stretch which is evidence of the progressive separation of the junctions. When the distance between the SWCNT increases beyond a critical distance, electrons can transfer only by hopping or tunneling from one tube to another because direct electronic transfer is impossible. These results suggest that the sensing mechanism was similar to that found for SWCNT paper embedded in PDMS.[25,27]

2.4. Deformable and Wearable Strain Sensors

To demonstrate the performance of the coaxial fibers as deformable sensors, we assembled eleven 4 cm long fibers to the back and front sides of a 70 cm long deformable, hollow cable (**Figure 4**), which could be manipulated into "strained," "S," and "circle" shapes. The sensors were attached to different locations on the cable using tape and the restriction of the cable motion was minimal. In the initial state, a metal rod was inserted into the hollow cable so that the strain on the coaxial fibers was 0% (Figure 4a,b). The initial resistance, R_0, was 200–300 Ω for all fibers. After removing the metal rod, the cable was extended and the coaxial fibers were in a "strained" state. The resistance of the fibers increased, corresponding to a strain of 10% (Figure 4b,c). The sensors on the back and front sides of the cable had similar $\Delta R/R_0$ in the uniaxial "strained" state, indicating that all sensors experienced the same level of strain. By manipulating the cable into "S" and "circle" shapes, the fibers on the two sides underwent asymmetrical deformation, leading to a dramatic difference between the $\Delta R/R_0$ of the curved inner and outer surfaces, as shown in Figure 4d,e. Moreover, it is possible to distinguish the shape of the cable through the 3D curves of the $\Delta R/R_0$ coordinates, proving that the coaxial fibers can be used as sensors for detecting and tracking the complicated movements of deformable objects.

We demonstrated the performance of our fibers to successfully sense motions on a deformable surface during the inflation of a balloon. We stuck sensors A, B, and C to the balloon at different locations, as shown in Figure 4f. We monitored the output signal from the fibers as the balloon was inflated from 12.6 to 14.6 cm two times, first with continuous air pressure, and then in six increments. The resistance data from the sensors, collected by IR-Bluetooth communication between a multimeter and a cellphone application, showed that the expansion of the balloon resulted in increased in resistance of the fibers (Figure 4g,h). Figure 4g,h clearly indicates that sensors A and B had the largest and smallest deformations, respectively. These results correspond to the different crack opening displacements of each sensor. The cracks opened faster under the uniaxial strain at sensor A, therefore the resistance change was larger than that of sensor B or C. Thus, we demonstrated that the fibers are able to differentiate the strain variation at different surface locations, indicating that they are able to be used as mechanical sensors for measuring strains on expandable surfaces.

We demonstrated the potential of our coaxial fibers in wearable electronics for sensor/human interface interactions, as shown in **Figure 5**. We attached two coaxial fibers with an epoxy adhesive (fibers 1 and 2 representing channels A and B, respectively) perpendicular to each other on a wristband (Figure 5a,b). Our sensor demonstrated reproducible ON/OFF switching with bending and relaxing motions of the wrist. Figure 5c shows that the $\Delta R/R_0$ of fiber 1 at 90° (channel A) is more obvious than the $\Delta R/R_0$ of fiber 2 at 0° (channel B). This result indicates that the sensor was able to detect motions at different locations on the wrist. The sensor also has the additional functionality of integration with textiles. By stitching the fibers into the sleeve of a jacket, we used them to create different signals for the motions of "pulling," "pressing," "folding," and "twisting."

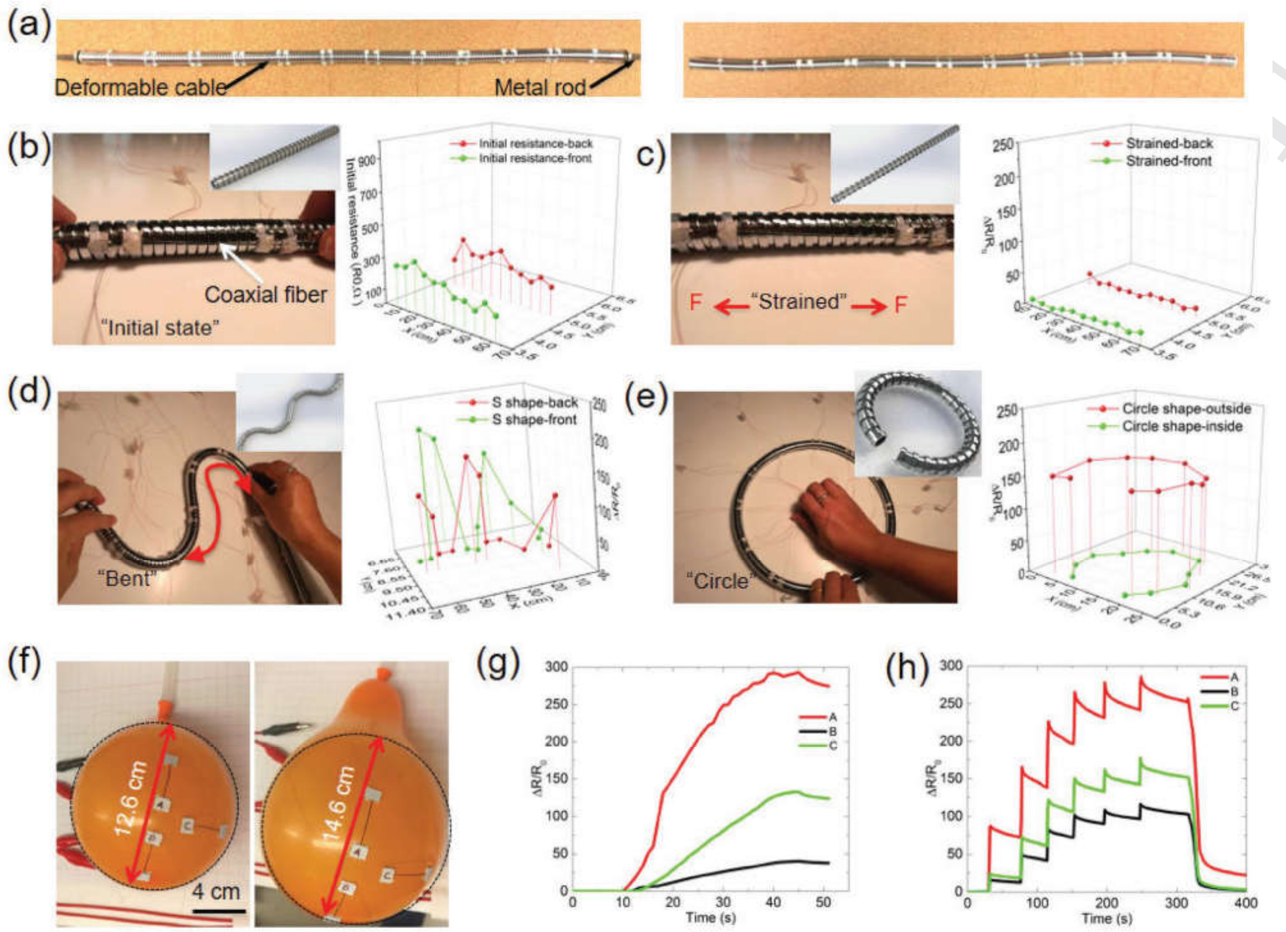

Figure 4. Demonstration of the coaxial fibers as deformable strain sensors. a) Photograph of a deformable cable in the initial and strained states. A metal stick inside the cable was used to keep it in the initial state. Eleven coaxial fibers were attached to each side of the cable. Photographs of the cable at b) initial, c) strained, d) bent, and e) circled conditions and the corresponding signal of resistance change. Insets in the images represent the model of the initial and deformed states of the cable. f) The initial and inflated state of a balloon attached three coaxial fibers. Three channels of resistance data were collected on a cell phone by a Meter Logger software using IR-Bluetooth communication. g,h) Relative change in resistance of the sensors under continuous and six steps of inflation of the balloon, respectively.

Thus, our sensor can also be used as a deformable and wearable mechanical sensors.

3. Conclusion

In conclusion, we demonstrated a coaxial wet-spinning and posttreatment approach to making coaxial fiber of thermoplastic elastomer-wrapped SWCNTs for high-performance strain sensors. The method is simple, industrially feasible, and applicable to conductive nanomaterials that cannot be wet-spun using previous methods. The coaxial fibers are highly stretchable and highly conductive. Owing to the coating of electrically insulative and highly stretchable thermoplastic elastomer, they are robust enough to be used as stretchable interconnects and as deformable and wearable strain sensors. The strain sensor based on our coaxial conductive fiber displayed several merits: (1) it combined high sensitivity, high stretchability, and high linearity; (2) the TPE sheath prevented short circuiting and ensured safe operation of the device; (3) the fibers demonstrated potential for large-scale production; and (4) the process for integration into wearable textiles was easy. One of the most interesting aspects of the technique is that the process is totally continuous and scalable. This study suggests that our coaxial fibers can find a wide range of applications in deformable and wearable electronic devices. Our strategy can be extended to other electrically conductive materials, e.g., carbon nanomaterials, metal nanoparticles, and conductive polymers, offering another approach to the next generation of deformable and wearable devices.

4. Experimental Section

Materials: SWCNTs functionalized with 2.7% carboxyl groups were purchased from CheapTubes, Inc., with over 90 wt% purity and containing more than 5 wt% of MWCNT. The true density of these SWCNTs was 2.1 g cm^{-3}.[24] Polystyrene-*block*-polyisoprene-*block*-polystyrene (TPE) (styrene, 22 wt%), methanesulfonic acid (CH_3SO_3H), ethanol, and dichloromethane (CH_2Cl_2) were purchased from Sigma-Aldrich.

Preparation of the SWCNT Dope and TPE Solution: A 2 wt% SWCNT dope was prepared by adding 0.2 g of SWCNTs into 9.8 g of $MeSO_3H$

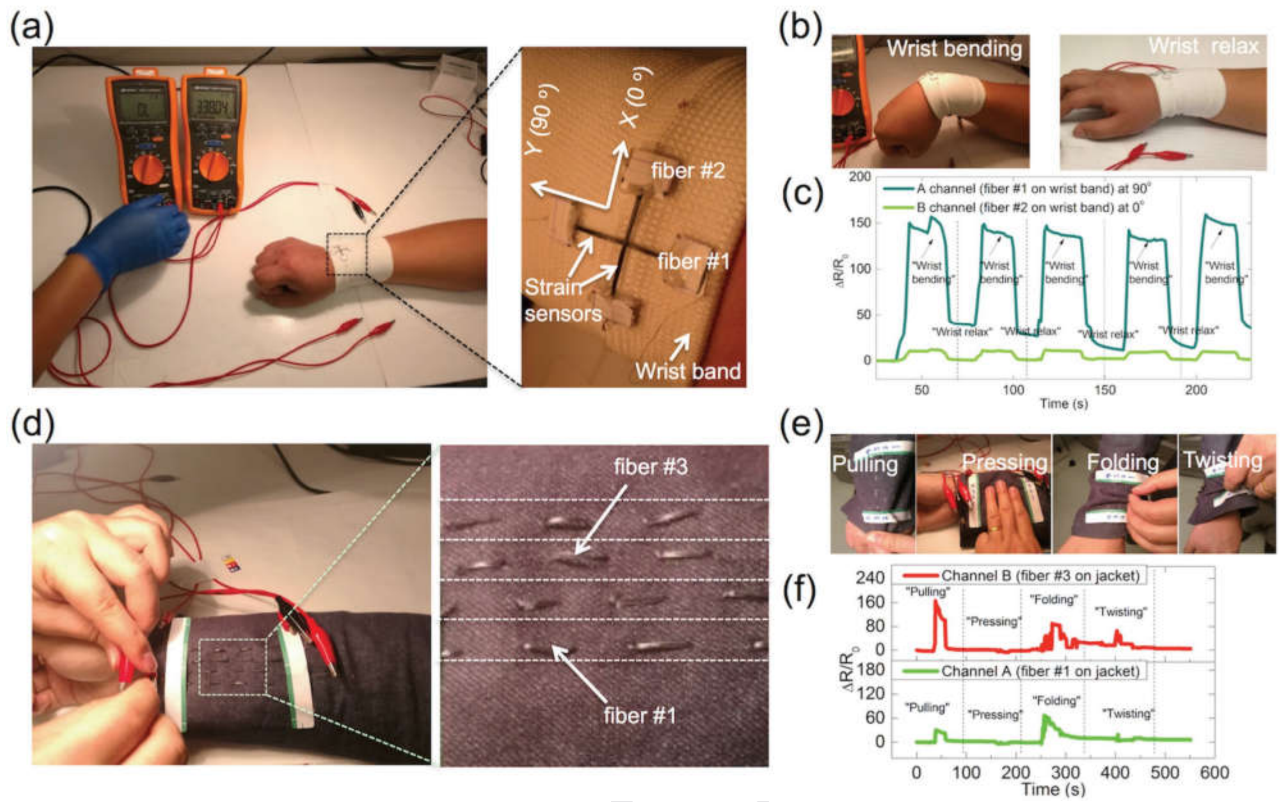

Figure 5. Applications of the coaxial fibers as wearable strain sensors. a) Photographs of the coaxial fibers attached to a wristband. Fibers 1 and 2 represent channels A and B, respectively. b) Bending and relaxing motions of the wrist. c) Relative change in resistance during wrist bending and relaxing. d) Photographs of the coaxial fibers stitched to the sleeve of a jacket. Fibers 1 and 3 represent channels A and B, respectively. The resistances of fibers 1 and 3 were monitored by multimeters. e) The "pulling," "pressing," "folding," and "twisting" motions applied to the coaxial fibers on the sleeve. f) The relative change in resistance corresponding with these motions.

and stirring for 2 min, followed by sonication using a Brason 8510 bath sonicator (250 W) (Thomas Scientific) for 60 min. The mixture was further stirred for 24 h, then pass through a 30 µm syringe filter (Pall Corporation) to remove aggregates. A 30 wt% TPE solution was prepared by mixing 9 g of TPE with 21 g of CH_2Cl_2 solvent at 200 rpm for 10 h.

Wet-Spinning of Coaxial Fibers: The SWCNT dope was loaded into a 10 mL syringe and spun into an ethanol bath at room temperature through an inner stainless steel needle (21 G). The flow rate of the ink was fixed at 150 µL min^{-1} by using a Fusion 200 syringe pump (Chemyx Inc.). The TPE solution in a 10 mL syringe was spun into the ethanol bath though an outer stainless steel needle (15 G). The flow rate of the ink was 200 µL min^{-1} . The fibers were continuously collected on a 50 mm winding spool, at a line speed of 2–4 m min^{-1}. Then, the fibers were soaked in an acetone bath for 6 h to remove the acid residue. The resulting fibers were removed from the acetone and densified by pressing with glass slides (Figure S3, Supporting Information). In detail, the fiber was taken out from acetone and simultaneously pressed by the glass slide, a large amount of residual acetone gradually evaporated with the pressing. This process leads to the deformation of the fiber from a tubular to a belt structure. The resulting deformation is permanent as a lot of acetone remains that enables the tubular structure to be reshaped. To confirm that acetone did not change the mechanical behavior of the fibers, it was determined that the coaxial fiber was able to sustain a stretch as high as 500% (Figure S4a, Supporting Information). For comparison of the mechanical properties, pure TPE fibers (Figure S5, Supporting Information) were prepared by wet-spinning of a 20 wt% TPE/DCM solution into the ethanol bath though a stainless steel needle (21 G) at an injection rate of 200 µL min^{-1}.

Characterizations: SEM was performed on the fibers using a Quanta 3D machine (FEI Company). The stretching and relaxing of the coaxial fibers were captured by a BX61 materials microscope (Olympus Corporation). FTIR spectra of pure TPE fibers before and after 6 h of washing with acetone were collected using a Nicolet iN10 spectrometer at 4 cm^{-1} resolution from an accumulation of 256 scans over the regions of 4000–650 cm^{-1}. The loading and unloading of the sample were controlled by a 5944 mechanical testing machine (Instron Corporation). Then, both ends of the 2 cm long fibers were dipped into colloidal silver ink, connected with copper wires, and painted with conductive silver epoxy. The resistance change of the fibers was monitored by a 34461A digital multimeter. The incremental, cyclic stretching and relaxing program were applied to initiate the fragmentation of the SWCNT core inside the coaxial fiber. The program was set to an incremental strain of 50%, starting at 0% and continuing until 250%, at a speed of 5 mm min^{-1}. Then, a cyclic stretching and relaxing program with maximum strains of 100% was applied at the same speed to the fibers for five cycles. The sensitivities of the strain sensors were defined as GF = $(\Delta R/R_0)/\varepsilon$, where R_0 is the initial resistance, $\Delta R/R_0$ is the relative change in resistance, and ε is the applied strain.[24,25]

For the EIS, the moduli of impedance, Z, and phase angle, θ, were measured with an Agilent E4980A Precision LCR meter in a two-probe configuration with Kelvin clips.[24,25] The frequency range was from 20 Hz to 2 MHz with a 1000 Hz step and a sweeping current of 50 mA. To understand the sensing mechanism of the fiber-based sensors, the change in impedance across a wide range of frequencies at different applied strains (0%, 5%, 15%, 20%, 40%, 60%, and 100%) was investigated.

Supporting Information

Supporting Information is available from the Wiley Online Library or from the author.

Acknowledgements

The research reported in this publication was supported by funding from King Abdullah University of Science and Technology (KAUST). The authors are grateful to KAUST for its support.

Conflict of Interest

The authors declare no conflict of interest.

Keywords

Q5 strain sensors, stretchable sensors, wearable electronics

Received: September 26, 2017
Revised: November 15, 2017
Published online:

[1] S. J. Benight, C. Wang, J. B. H. Tok, Z. A. Bao, *Prog. Polym. Sci.* **2013**, *38*, 1961.
[2] J. P. Li, S. H. Qi, J. J. Liang, L. Li, Y. Xiong, W. Hu, Q. B. Pei, *ACS. Appl. Mater. Interfaces* **2015**, *7*, 14140.
[3] J. Park, I. You, S. Shin, U. Jeong, *ChemPhysChem* **2015**, *16*, 1155.
[4] D. J. Lipomi, *Adv. Mater.* **2016**, *28*, 4180.
[5] H. S. Kang, H. T. Kim, J. K. Park, S. Lee, *Adv. Funct. Mater.* **2014**, *24*, 7273.
Q6 [6] H. H. Chou, A. Nguyen, A. Chortos, J. W. F. To, C. Lu, J. G. Mei, T. Kurosawa, W. G. Bae, J. B. H. Tok, Z. A. Bao, *Nat. Commun.* **2015**, *6*.
[7] Z. Y. Liu, D. P. Qi, P. Z. Guo, Y. Liu, B. W. Zhu, H. Yang, Y. Q. Liu, B. Li, C. G. Zhang, J. C. Yu, B. Liedberg, X. D. Chen, *Adv. Mater.* **2015**, *27*, 6230.
[8] W. Zeng, L. Shu, Q. Li, S. Chen, F. Wang, X. M. Tao, *Adv. Mater.* **2014**, *26*, 5310.
[9] S. Zhu, J. H. So, R. Mays, S. Desai, W. R. Barnes, B. Pourdeyhimi, M. D. Dickey, *Adv. Funct. Mater.* **2013**, *23*, 2308.
[10] L. Kou, T. Q. Huang, B. N. Zheng, Y. Han, X. L. Zhao, K. Gopalsamy, H. Y. Sun, C. Gao, *Nat. Commun.* **2014**, *5*.
[11] Z. F. Liu, S. Fang, F. A. Moura, J. N. Ding, N. Jiang, J. Di, M. Zhang, X. Lepro, D. S. Galvao, C. S. Haines, N. Y. Yuan, S. G. Yin, D. W. Lee, R. Wang, H. Y. Wang, W. Lv, C. Dong, R. C. Zhang, M. J. Chen, Q. Yin, Y. T. Chong, R. Zhang, X. Wang, M. D. Lima, R. Ovalle-Robles, D. Qian, H. Lu, R. H. Baughman, *Science* **2015**, *349*, 400.
[12] Y. Cheng, W. R., S. J., L. Gao, *Adv. Mater.* **2015**, *27*, 7365.
[13] M. Amjadi, K. Kyung, I. Park, M. Sitti, *Adv. Funct. Mater* **2016**, *26*, 1678.
[14] Q. Cao, J. A. Rogers, *Adv. Mater.* **2009**, *21*, 29.
[15] C. Y. Wang, X. Li, E. L. Gao, M. Q. Jian, K. L. Xia, Q. Wang, Z. P. Xu, T. L. Ren, Y. Y. Zhang, *Adv. Mater.* **2016**, *28*, 6640.
[16] J. Ge, L. Sun, F. R. Zhang, Y. Zhang, L. A. Shi, H. Y. Zhao, H. W. Zhu, H. L. Jiang, S. H. Yu, *Adv. Mater.* **2016**, *28*, 722.
[17] J. Zhou, E. Q. Li, R. Li, X. Xu, I. Aguilar Ventura, A. Moussawi, D. Anjum, M. N. Hedhili, D. Smilgies, G. Lubineau, S. T. Thoroddsen, *J. Mater. Chem. C* **2015**, *3*, 2528.
[18] J. Zhou, M. Mulle, Y. B. Zhang, X. Z. Xu, E. Q. Li, F. Han, S. T. Thoroddsen, G. Lubineau, *J. Mater. Chem. C* **2016**, *4*, 1238.
[19] J. Zhou, Y. Zhang, M. Mulle, G. Lubineau, *Meas. Sci. Technol.* **2015**, *26*, 085003.
[20] H. Miura, Y. Fukuyama, T. Sunda, B. Lin, J. Zhou, J. Takizawa, A. Ohmori, M. Kimura, *Adv. Eng. Mater.* **2014**, *16*, 550.
[21] S. Lee, S. Shin, S. Lee, J. Seo, J. Lee, S. Son, H. J. Cho, H. Algadi, S. Al-Sayari, D. E. Kim, T. Lee, *Adv. Funct. Mater.* **2015**, *25*, 3114.
[22] A. J. Granero, P. Wagner, K. Wagner, J. M. Razal, G. G. Wallace, M. I. H. Panhuis, *Adv. Funct. Mater.* **2011**, *21*, 955.
[23] S. Seyedin, J. M. Razal, P. C. Innis, A. Jeiranikhameneh, S. Beirne, G. G. Wallace, *ACS Appl. Mater. Interfaces* **2015**, *7*, 21150.
[24] J. Zhou, X. Xu, Y. Hu, G. Lubineau, *Nanoscale* **2017**, *9*, 604.
[25] J. Zhou, Y. Hu, X. Xu, F. Han, G. Lubineau, *ACS Appl. Mater. Interfaces* **2017**, *9*, 4835.
[26] W. Shi, N. A. Lynd, D. Montarnal, Y. D. Luo, G. H. Fredrickson, E. J. Kramer, C. Ntaras, A. Avgeropoulos, A. Hexemer, *Macromolecules* **2014**, *47*, 2037.
[27] Y. Xin, J. Zhou, G. Xu, X. and Lubineau, *Nanoscale* **2017**, *9*, 10897.
[28] J. T. Muth, D. M. Vogt, R. L. Truby, Y. Menguc, D. B. Kolesky, R. J. Wood, J. A. Lewis, *Adv. Mater.* **2014**, *26*, 6307.
[29] X. Q. Liao, Q. L. Liao, Z. Zhang, X. Q. Yan, Q. J. Liang, Q. Y. Wang, M. H. Li, Y. Zhang, *Adv. Funct. Mater.* **2016**, *26*, 3074.